

THE FREQUENCY AGILE SOLAR RADIOTELESCOPE

DALE E. GARY¹

¹Center for Solar-Terrestrial Research, NJIT, University Heights, Newark, NJ 07102, USA

E-mail: dgary@njit.edu

ABSTRACT

Solar radio astronomy is about to undergo a revolution with the advent of a new radio synthesis array, the Frequency Agile Solar Radiotelescope (FASR). The array will consist of more than 100 antennas (5000 baselines), and will be designed to meet the special challenges of solar imaging. It will produce high-quality images at hundreds of frequencies in the range 20 MHz–24 GHz. We briefly describe the plans for the instrument, and then concentrate on the range of science that is expected to be addressed, using current state-of-the-art solar radio observations and modeling to illustrate FASR performance. We end with an assessment of the current status of the instrument, and plans for future.

Key words : Sun: magnetic fields—Sun: radio radiation—Sun: corona

I. INTRODUCTION

Studies of the Sun have been undertaken over a wide range of radio wavelengths utilizing many dissimilar instruments built for many different purposes. These include imaging instruments at a few widely spaced frequencies, such as the Very Large Array (VLA), the Nobeyama Radioheliograph (NoRH), and the Nancay Radioheliograph (NRH). There are also instruments with good spectral resolution but limited spatial resolution or imaging capability, such as the Owens Valley Solar Array (OVSA), and the RATAN 600. Yet the range of solar physics addressable through radio emission is extremely broad, by virtue of the simplicity of the main emission processes (those due to incoherent emission from electrons), the strong dependence of the emission on magnetic field strength, and the many decades of frequency available in the radio range. No single existing instrument comes close to the combination of spatial resolution, image quality, spectral resolution, wide spectral coverage, and time resolution that is needed to fully exploit the power of solar radio emission diagnostics.

However, recent advances in broadband devices, digital circuitry and computing power have made it feasible to design an instrument at modest cost that will have this challenging combination of capabilities. We are currently in the design stage of just such an instrument, called the Frequency Agile Solar Radiotelescope (FASR). FASR is envisioned as a solar-dedicated interferometer array capable of producing high-resolution, high-fidelity, and high-dynamic-range images over an extremely broad frequency range of ~ 0.02 –24 GHz, and thus will provide imaging spectroscopy of the full disk of the Sun with up to 0.1 s time resolution. Various aspects of the FASR project appear elsewhere in the literature (Bastian 2003*a, b*; White et al. 2003; Gary & Keller 2003).

The Sun is spatially and temporally complex. The Sun's radio brightness can change by orders of magni-

tude on extremely short timescales. Hence, the usual technique of Earth rotation aperture synthesis that is used to improve the image quality of cosmic sources, which are essentially unchanging in time, does not work with the Sun. Instead, a large number of visibility measurements must be made instantaneously, requiring a large number of antennas. For an array of N antennas, there are $N(N - 1)/2$ antenna pairs. The image quality desired for FASR will require ~ 100 antennas, giving ~ 5000 instantaneous visibility measurements. This “snapshot” imaging approach is used superbly by Japan's NoRH at two frequencies, but FASR will achieve it at hundreds of frequencies.

We present the basic FASR instrument design in §2. In §3 we present some highlights of the broad science to be addressed by FASR. We conclude in §4 with a discussion of the current status and plans for the future.

II. BASIC DESIGN OF FASR

The FASR instrument specifications were developed at several meetings involving the international solar and radio physics communities encompassing at least 8 years of study. With funding from the U.S. National Science Foundation and NASA, we convened the FASR Science Definition Workshop at the National Radio Astronomy Observatory (NRAO) in Green Bank, WV, in May 2002, followed by a smaller FASR Technical Workshop held at the NRAO in Charlottesville, VA, in August 2002. Consideration of key science goals and the relevant radio emission mechanisms yielded the instrument requirements summarized in Table 1.

The specifications are broken into different frequency ranges because it is not possible to cover the entire, almost three decades in frequency with a single antenna system. Currently we envision three separate antenna systems, comprising 2-m antennas at the high frequency end, 6-m antennas in the intermediate range from 0.25–3 GHz, and an array of log-periodic dipoles (LFA) at the low-frequency end. The selection of an-

Table 1. FASR Instrument Specifications

Angular resolution	$20/\nu_{\text{GHz}}$ arcsec
Frequency range	$\sim 0.1\text{-}24$ GHz
Frequency resolution	< 3 GHz: 0.1% > 3 GHz: 1%
Time resolution	< 3 GHz: 10 ms > 3 GHz: 100 ms
Polarization	Stokes I & V
Number antennas	2-24 GHz: 100 0.25-3 GHz: 60 < 0.3 GHz: 40
Size antennas	2-24 GHz: 2 m 0.25-3 GHz: 6 m < 0.3 GHz: LFA
Maximum antenna spacing	6 km
Absolute positions	1 arcsec
Absolute flux calibration	$< 5\%$
ΔT_B	(snapshot) 1000 K

tenna sizes is based on the desire to cover the entire Sun at as high a frequency as possible (to ~ 18 GHz with a 2 m antenna), together with the growing inefficiency of dishes at low frequencies, which cease to work effectively at diameters $D/\lambda \approx 5$.

The angular resolution of the array will be determined by the maximum projected spacing of antennas, which is of order 6 km in order to maintain the required $1''$ resolution at 20 GHz over ± 3 h. The spatial resolution scales linearly with frequency, so that it is $2''$ at 10 GHz, $4''$ at 5 GHz, and $20''$ at 1 GHz. These resolution limits are a good match to the natural and unavoidable scattering of radio emission in the coronal plasma (see Bastian 1994). A possible array configuration is shown in Figure 1.



Fig. 1.— Artists conception of the FASR array of 2-m and 6-m antennas, in a spiral configuration, as they may appear at a site near the VLA in New Mexico. The LFA elements are not shown.

The array configuration shown in Figure 1 is a log-spiral configuration that has self-similar scaling, so that the range of spatial scales is identical for different subsets of antennas at different frequencies (Sault & Conway 1999; Bastian et al. 1998). However, the snapshot coverage using all antennas is not necessarily optimum. There are algorithms now available that can determine a nearly optimum configuration (minimizing sidelobes or optimizing the corresponding u, v distribution) by randomly shifting antennas from their initial locations until the desired constraint is reached (e.g. Boone 2001). More configuration studies are needed. However, FASR’s imaging properties are excellent even with the self-similar array configuration. Figure 2, from Bastian (2003*b*), shows the snapshot imaging fidelity of a 102 element, three-armed, log-spiral array.

The frequency and time resolution specifications listed in Table 1 are based on observed characteristics of solar phenomena in the different frequency ranges, which vary considerably across the broad radio spectrum. At frequencies > 3 GHz, both thermal and non-thermal incoherent mechanisms dominate, but moderate 1% spectral resolution is still required to resolve the abrupt brightness changes due to gyroresonance. At lower frequencies, coherent emission mechanisms become important, which requires somewhat higher temporal and spectral resolution.

FASR must make accurate measurements of at least the Stokes I and V polarization parameters. The Stokes Q and U parameters are not relevant, in most cases, because strong differential Faraday rotation in the solar corona washes out any intrinsically linearly polarized radiation, but the instrument will be able to measure them, and we plan to retain the option of recording them on an occasional basis for certain exploratory investigations.

FASR will be calibrated against cosmic standards with secondary calibration against geostationary satellites at selected frequencies. We expect to be able to make snapshot maps with an rms brightness of 1000 K or less. A modest amount of frequency synthesis will be possible and desirable for many types of programs. These will yield significantly lower rms brightness variations.

III. FASR SCIENCE GOALS

The radio emission at different frequencies broadly corresponds to different heights in the solar atmosphere, so that the nearly three decades in frequency correspond to a height range from the chromosphere to about 1 solar radius above the surface. This gives a kind of CAT-scan quality to the FASR dataset, which can be exploited to study the wide variety of structures and phenomena that occur in this height range. The sensitivity of the radio emission mechanisms to both thermal and nonthermal emission, wave-particle interactions, and plasma parameters such as magnetic field, temperature and density give FASR unique diagnostic

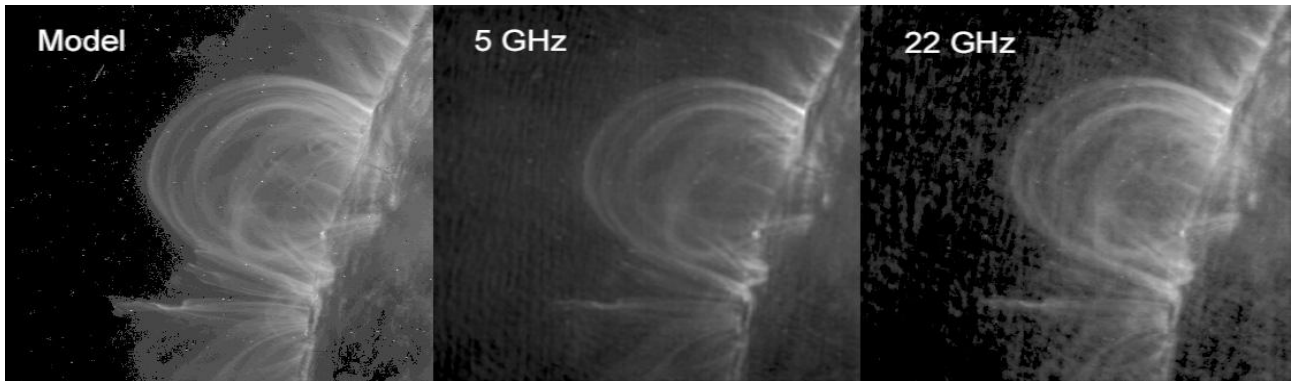


Fig. 2.— Simulation of the imaging properties of a log-spiral array. *a)* model image from TRACE, 6 Nov 1999; *b)* snapshot image made at 5 GHz; *c)* snapshot image made by same array at 22 GHz. The instrument response function has not been deconvolved from the snapshot maps. From Bastian (2003*b*)

tools to address a large number of outstanding problems in solar physics. The highlights are:

- the nature and evolution of coronal magnetic fields
- the physics of flares
- drivers of space weather
- the quiet Sun

These will be discussed in more detail in this section.

(a) Coronal Magnetic Fields

The magnetic fields of the solar atmosphere are the key player in all of solar activity, yet they remain largely inaccessible to direct measurement. Although radio emission has long had the potential to make measurements of the coronal field, the required combination of spatial and spectral resolution has been lacking. FASR is specially designed to exploit the diagnostic potential of radio emission by focusing on high-quality spectroscopic imaging.

As a result, true coronal magnetograms will be a standard data product of the instrument. The observational and theoretical underpinnings of the technique have been reported in many papers, e.g. Gary & Hurford (1994), Lee et al. (1998), Brosius et al. (2002), White & Kundu (1998). To illustrate the power of FASR to produce such magnetograms, we have done simulations of a complex active region model, provided by Y. Mok, as described in Mok et al. (2003). We have calculated the radio emission produced by both the gyroresonance and free-free mechanisms at 100 frequencies from 1-24 GHz, and then analyzed the resulting images to deduce the magnetic field strength. The deduced magnetic field parameters can then be compared directly with the model field to assess the precision of the measurements.

The upper two panels of Figure 3 show the magnetic field and the temperature at coronal heights for the model. The lower two panels show the simulated

images at two frequencies, after passing through the instrumental sampling function based on a log-spiral antenna configuration. The brightness distribution is due to the combination of coronal temperature and opacity variations, both of which are quite complicated for this complex model. Interpreting images at a few widely-spaced frequencies is impossible due to this complexity, but when images at 100 frequencies are available, the spatially resolved spectra at each point in the maps can be interpreted precisely and uniquely.

Example spectra for two lines of sight are shown in Figure 4 for the two circular polarizations (solid line is RCP, and dashed line is LCP). The abrupt drop in brightness in both modes of polarization is due to the temperature transition from coronal temperatures to chromospheric temperatures, and the frequency at which the drop occurs is directly proportional to the magnetic field through the gyroresonance equation

$$f = s f_B = \frac{seB}{2\pi mc} = 2.8 \times 10^6 sB \quad (1)$$

where f_B is the gyrofrequency and s is the relevant harmonic for the emission, which is an integer value to be determined. For conditions of the solar corona, the relevant harmonic is typically $s = 2$ or $s = 3$, although the examples in Fig. 4 are chiefly $s = 1$ and $s = 2$. The method allows the direct determination of the *magnetic field strength* and the polarity (from the dominance of one circular polarization over the other), but not the vector field. Such spectra as in Figure 4 are available at every resolution element in the maps, so that the magnetic field can be uniquely determined everywhere in the active region.

Figure 5 shows a comparison of the deduced magnetic fields with the actual fields in the model, at a height of about 500 km. The comparison shows excellent quantitative agreement, and demonstrates that the method works as expected, even for a complex active region. We are working on a more sophisticated algorithm for fitting the spectra, to avoid the gaps shown

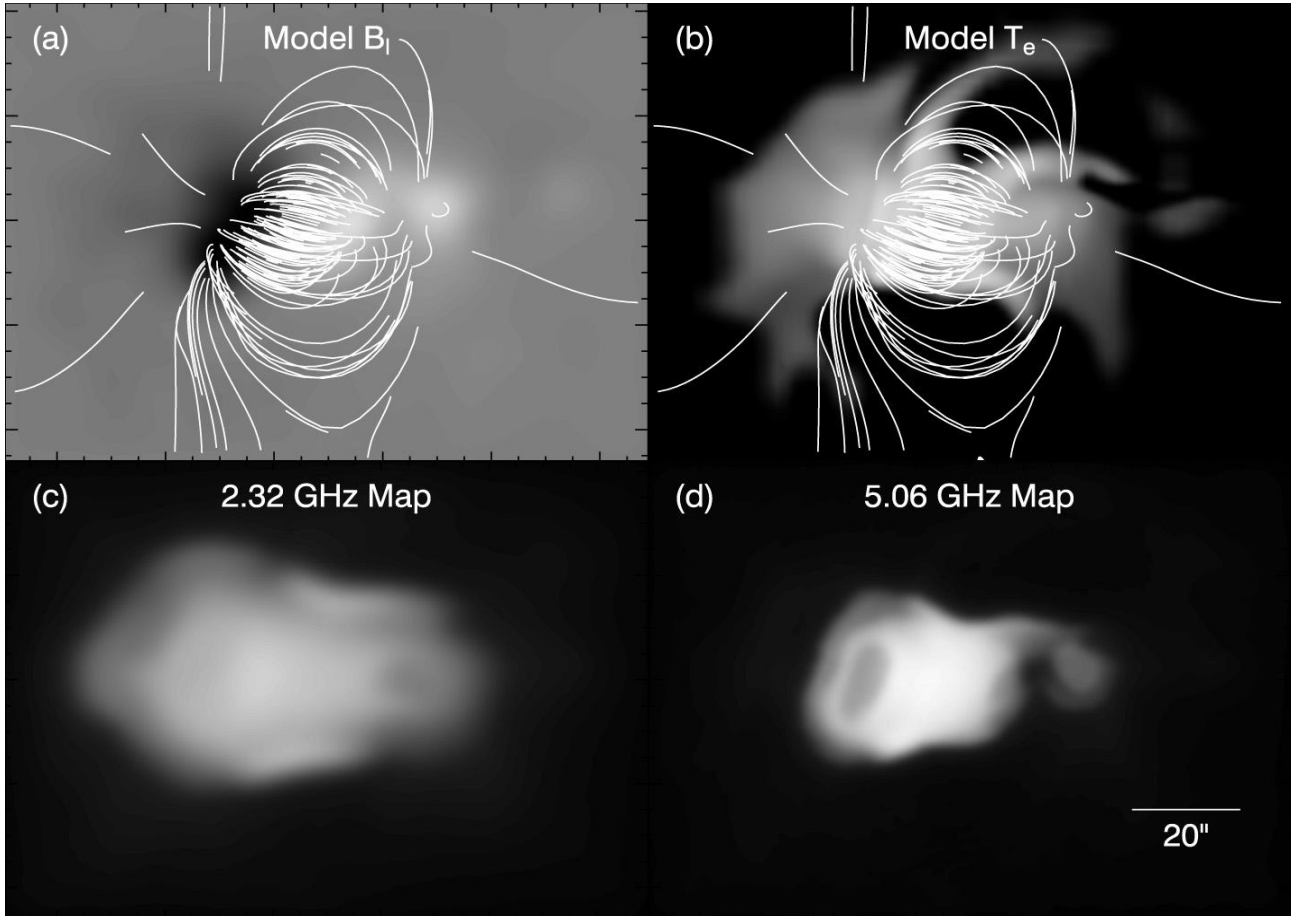


Fig. 3.— (a) Longitudinal field strength in the model, at a height of 1000 km, overlaid with field lines calculated from the model. The longitudinal field ranges from -1482 G (black) to 1102 G (white). (b) Electron temperature at the same height, again overlaid with field lines. The temperature at this height ranges from 21000 K (black) to 2.17 MK (white). (c) The calculated radio emission at a frequency of 2.32 GHz. (d) The calculated radio emission at a frequency of 5.06 GHz.

in Fig. 5.

We mention in passing that the spectra in Figure 4 show not only the magnetic signature due to gyroresonance emission, but also polarization due to magnetic fields in the free-free emission component, which can be seen at frequencies $> 3f_B$. Model calculations show that it is possible to exploit this dependence as well, to obtain longitudinal magnetic field measurements in the quiet Sun using the inversion techniques of Grebinskij et al. (2000). This is an observational challenge for FASR, and the implications for FASR design are now being studied.

(b) The Physics of Flares

FASR will be designed to obtain well-calibrated data on the short time scales and the vast brightness range encompassed by solar flares. The broad frequency coverage will allow us to gain fundamental new insights into flare buildup, initial energy release, and subsequent transport and thermalization of electrons accelerated in

flares. The simultaneous coverage of CMEs (see next section) and flare processes should allow us to better understand the connection between these two complex phenomena.

Although we can identify tracers of energy release in the solar corona with spectrographs (see Bastian, Benz, & Gary 1998 for a review), the relevant range of frequencies (the decimetric range, especially ~ 400 -1000 MHz) has never been explored with high-resolution imaging observations. This frequency range corresponds to densities of $2\text{-}8 \times 10^9 \text{ cm}^{-3}$, densities where energy release in flares is thought to occur. As illustrated in Figure 6, from Aschwanden & Benz (1997), decimetric type III bursts (III_{dm}), due to plasma radiation excited by electron beams, are seen to start around 500 MHz and drift to both higher and lower frequencies, indicating both upward and downward propagating beams. Many such bursts are typically released during the course of the impulsive phase of a flare and are believed to be intimately related to energy release in flares via magnetic reconnection. FASR will image

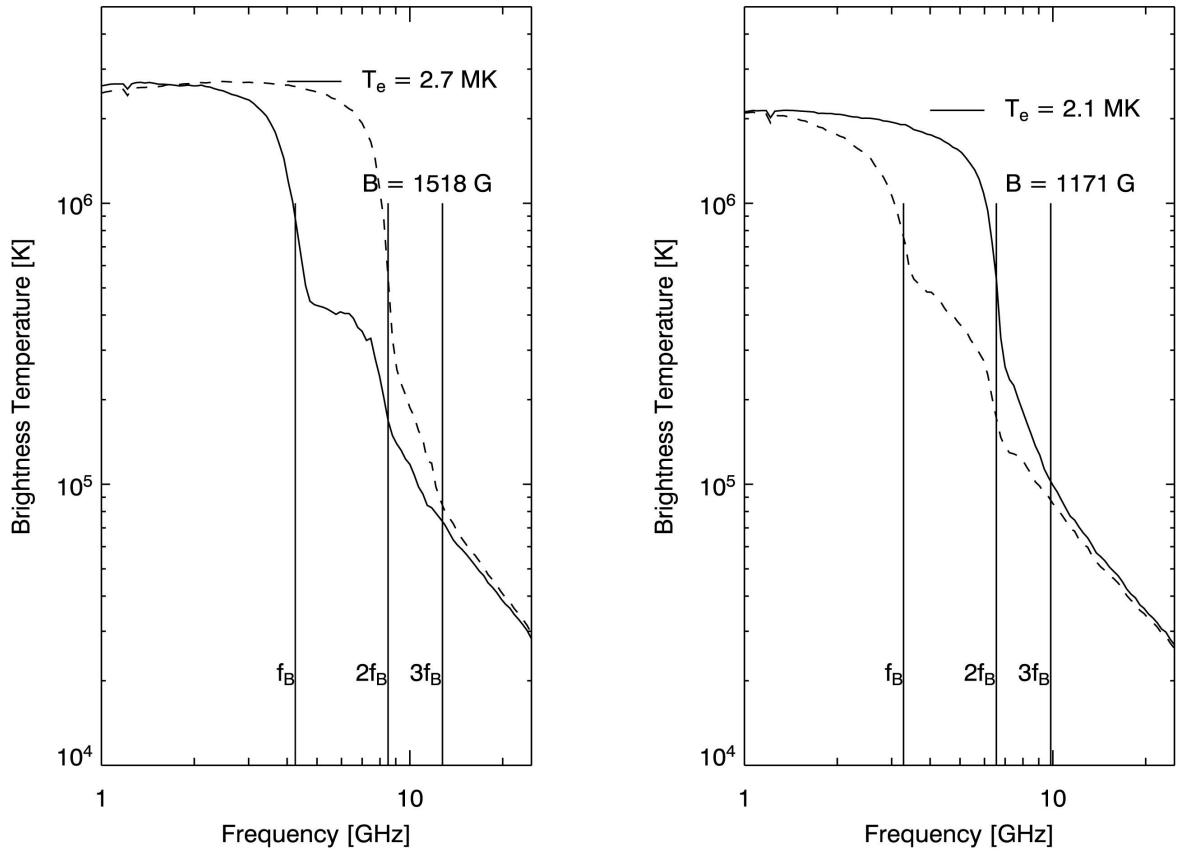


Fig. 4.— The right-hand circular polarization (RCP, solid curve) and left-hand circular polarization (LCP, dashed curve) radio emission spectra at two lines of sight in the active region, as calculated at 100 frequencies from 1-24 GHz, after folding through the instrumental response. The electron temperature of the corona can be read directly from the spectra at low frequencies, where the emission is optically thick. The frequency at which abrupt drops in brightness occur are identified with different harmonics of the gyrofrequency (vertical lines), allowing the magnetic field strength to be unambiguously determined.

these bursts for the first time, and the change of source location with frequency will pinpoint the location of the reconnection as well as the trajectory of the field lines above and below the reconnection point.

Fig. 6 also shows the schematic relationships among the different structural components of a flare, e.g. the soft X-ray loops, the hard X-rays and H-alpha ribbons at footpoints, and the microwave emitting loops, which are typically sites of enhanced trapping of electrons. Incoherent gyrosynchrotron radiation from a nonthermal population of such energetic electrons is responsible for the bulk of the radio emission in flares. The spectrum and polarization of the radiation is sensitive to the details of the electron distribution function, including the spectral index of the power-law tail, the presence of a high-energy cutoff, and the degree of anisotropy. Imaging spectroscopy of the flaring source can therefore be used to infer the electron distribution function as a function of time and space in the flare source, offering

new insights into electron acceleration and transport processes. For example, it should be possible to establish the relationship between directly precipitating electrons seen in hard X-rays and trapped electrons in the coronal volume. FASR data should spur sophisticated theoretical and modeling studies concerning electron scattering, whether dominated by Coulomb collisions or wave-particle interactions. In addition, the microwave spectrum depends sensitively on the local vector magnetic field and the ambient plasma density. Thus, the magnetic field strength and direction will be two parameters that will be highly constrained as a function of position in the flaring loops, along with the ambient plasma density.

One of the outstanding and unique capabilities of FASR will be to provide an integrated picture of the solar atmosphere at both high and low energy during solar flares, from the mid-chromosphere to a solar radius or more above the surface. This will give a system-wide

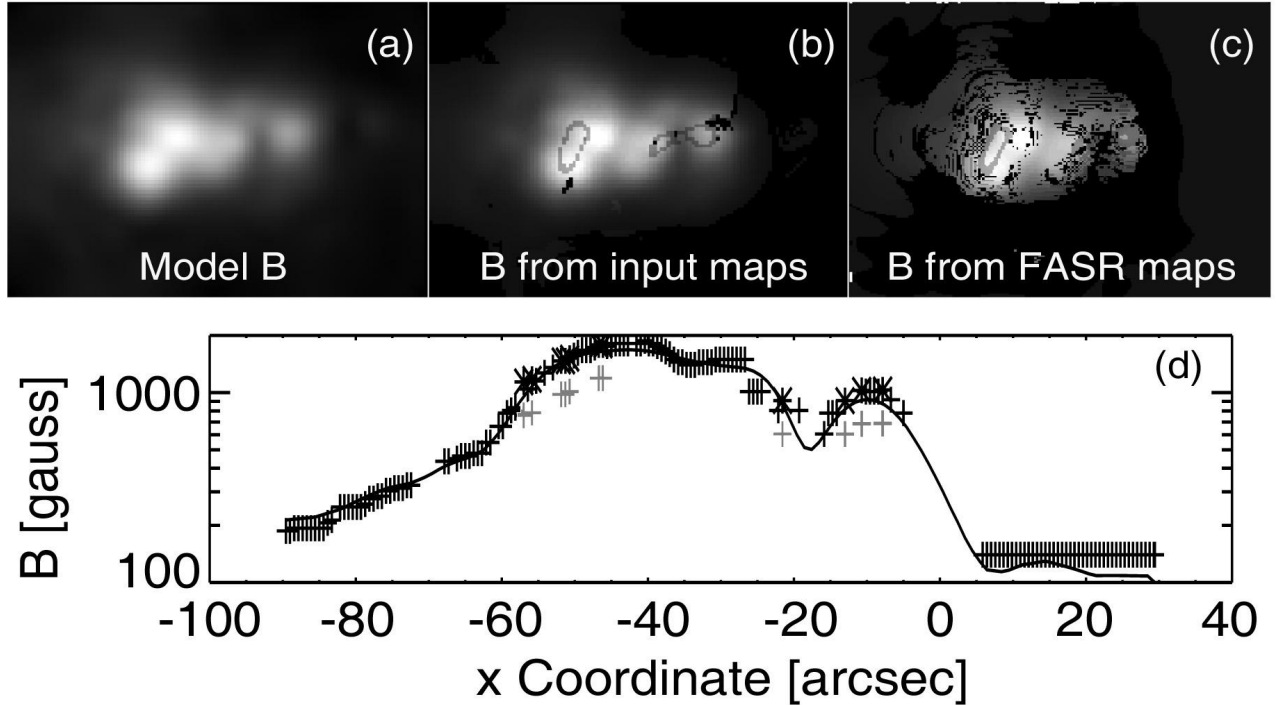


Fig. 5.— A demonstration of one method of determining magnetic field strength from radio spectra such as in Fig. 4. (a) The total magnetic field strength from the model, at a height of about 500 km, for comparison. (b) A magnetic field map deduced from the “perfect” radio spectra calculated from the model, before folding it through the instrument response. A simple automatic procedure was used to find the sharp brightness drops in the spectra, as illustrated in Fig. 4, at every point in the maps. The points of obviously weaker B (gray contour-like patterns) are points where the relevant harmonic in equation (1) was assumed to be $s = 3$, but is really $s = 2$. Such errors are obvious and can be corrected with a slightly more complex procedure. The black pixels are points where the algorithm failed. (c) A magnetic field map deduced from the radio maps after folding through the instrument response. Where the simple algorithm works, the results are excellent, as shown in the comparison in panel *d*, except for correctable errors in harmonic number. (d) A profile of B across the center of the maps, for quantitative comparison. The solid curve is the model B , while the crosses are the corresponding fits from *c*. The gray crosses are points of error in harmonic number, which after correction by a factor 1.5 become the asterisks.

view of energy release, electron acceleration, electron transport, plasma heating, and associated phenomena. Coupled with observations from other ground- and space-based solar instruments, FASR will help to revolutionize our understanding of flare energy release.

(c) Drivers of Space Weather

FASR will address the solar origins of space weather, through its panoramic view of the solar atmosphere over the relevant height range. This includes imaging both thermal and nonthermal emissions from Coronal Mass Ejections (CMEs), tracking the trajectories of electron beams (type III radio bursts), imaging of shock waves (type II radio bursts), and context imaging of other associated emissions such as type IV storm emission. In addition, FASR may play a significant programmatic role in forecasting and “nowcasting” events, and in providing near real-time data products of interest to the space weather community.

Bastian and Gary (1997) examined the expected thermal emission from CMEs due to thermal free-free emission, and concluded that the decimetric range below ~ 900 MHz might be the best in terms of contrast of the CME against other coronal and burst emissions. The density enhancement of the CME itself is expected to provide sufficient optical depth to make the CME visible against the disk. Spectral measurements of such radiation can provide density and temperature diagnostics within the CME. Observations of the thermal signature of CMEs from existing instruments are rare (Gopalswamy & Kundu 1992; Kathiravan et al. 2002) due to limited dynamic range and the fact that the observing frequency is not optimum. FASR will make high dynamic range images in the appropriate frequency range, with reasonable spatial resolution of order $30''$. In addition to the thermal emission, recent observations from the Nancay Radioheliograph (Bastian et al. 2001) have succeeded in directly imaging nonthermal gyrosynchrotron emission from CMEs at multiple

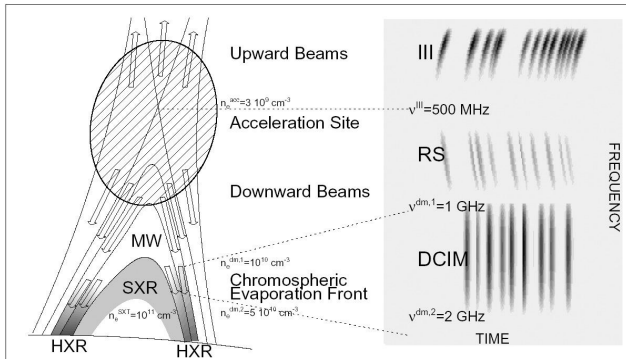


Fig. 6.— A schematic representation of a typical flaring loop geometry (left panel), and the corresponding dynamic spectrograph features (right panel) that may result. The frequency around 500 MHz corresponds to the height range in the corona where the reconnection and acceleration often occur. Figure from Aschwanden & Benz (1997).

frequencies. Figure 7 (left panel) shows the expanding CME loops at 164 MHz (emission from the background Sun has been subtracted). The right panel shows model fits to multi-point spectra at several lines of sight along the loop, at the points indicated in the left panel. Such nonthermal gyrosynchrotron radiation gives quantitative diagnostics of magnetic field strength. In this case the changing spectrum with position along the loop is modified by Razin-Tsytovich suppression, which gives a constraint on the ratio of density to magnetic field strength. Modeling allows both parameters to be estimated. The field strength in this case ranged from 1.47 G (position 1 in Figure 7) to 0.33 G (position 4), as described by Bastian et al. (2001).

Other signatures of eruptive phenomena, including CMEs, are also accessible by FASR observations. For example, White (priv. comm., 2002) has an image sequence showing the radio analog to “EIT waves” observed at 17 GHz with the Nobeyama Radioheliograph. FASR’s frequency coverage will provide brightness temperature spectra of such features, from which densities and temperatures can be deduced. Such observations offer the means of probing the birth and acceleration of erupting filaments, CMEs and wave disturbances both on the disk and off the limb.

FASR will also be an extremely powerful instrument for relating type II radio bursts to other associated activity such as flares and CMEs. At present it is controversial whether metric type II bursts are the same as their interplanetary counterparts (Cane & Reames 1988). Gary et al. (1984) showed from spatially resolved radio observations that the type II burst had to be embedded within CME loops, since the requisite densities existed only there. The mechanism by which shocks accelerate electrons, and the conditions required for them to do so, is still largely unknown due in part to the scant observational data with spatial resolution. FASR will provide excellent, high-dynamic range imag-

ing, but most importantly it will do so over a wide range of closely spaced frequencies. Since any one part of the shock only emits over a limited range of frequencies, this spectral coverage is needed to determine the overall size and shape of the emitting source. Trajectories of type III-like SA events (Cane & Stone 1984) streaming away from the shock will help define the magnetic topology of the part of the shock most efficient at accelerating electrons. Such observations will provide a much needed observational basis for understanding solar energetic particle (SEP) events.

(d) Quiet Sun

The temperature, density and magnetic field structure of the quiet Sun, both at the chromospheric and coronal levels, remains a mystery despite decades of study. The magnetic fields are observed to be concentrated into the network structure due to supergranular fluid motions, but questions remain about the nature of interactions among these magnetic field elements, how the field expands into the corona (magnetic canopy), and what the implications of the magnetic structure and dynamics are for the temperature and density structure of the chromosphere and corona. High-resolution radio images of the network (Gary & Zirin 1988; Gary, Zirin & Wang 1990; Bastian, Dulk & Leblanc 1996) reveal that the contrast between network and intranetwork regions is many thousands of kelvin, with interesting structural changes with frequency. FASR will provide high-resolution images at many frequencies that will give a CAT-scan-like sensitivity to the atmospheric structure in exactly the height range in the upper chromosphere where the interesting structural changes are expected. From other radio observations we already have hints of interesting differences in coronal holes and ordinary quiet Sun in this height range. For instance, at 17 GHz polar holes are brighter than the mean quiet Sun (Nindos et al. 1999; Shibasaki 1998), while at frequencies near 5 GHz and below they appear dark, as in soft X-rays. This indicates a perhaps significant difference in temperature and density structure in holes as compared to ordinary quiet Sun, but only with the continuous spectrum that FASR will provide can we expect to invert the data to deduce the atmospheric structure. Such measurements might offer a clue to acceleration of the high speed solar wind from coronal holes.

Numerous radio observations also show that the chromospheric network structure is highly dynamic. Gary & Zirin (1988) discussed significant changes in structure on the timescale of hours, while Krucker et al. (1997) show numerous small scale brightenings on much shorter timescales. The models of Carlsson & Stein (1995) suggest that the entire chromospheric structure is so dominated by dynamical changes that an average structure ceases to have meaning. FASR will have the capability to image the quiet Sun, but such imaging over the entire disk is a great challenge due to the

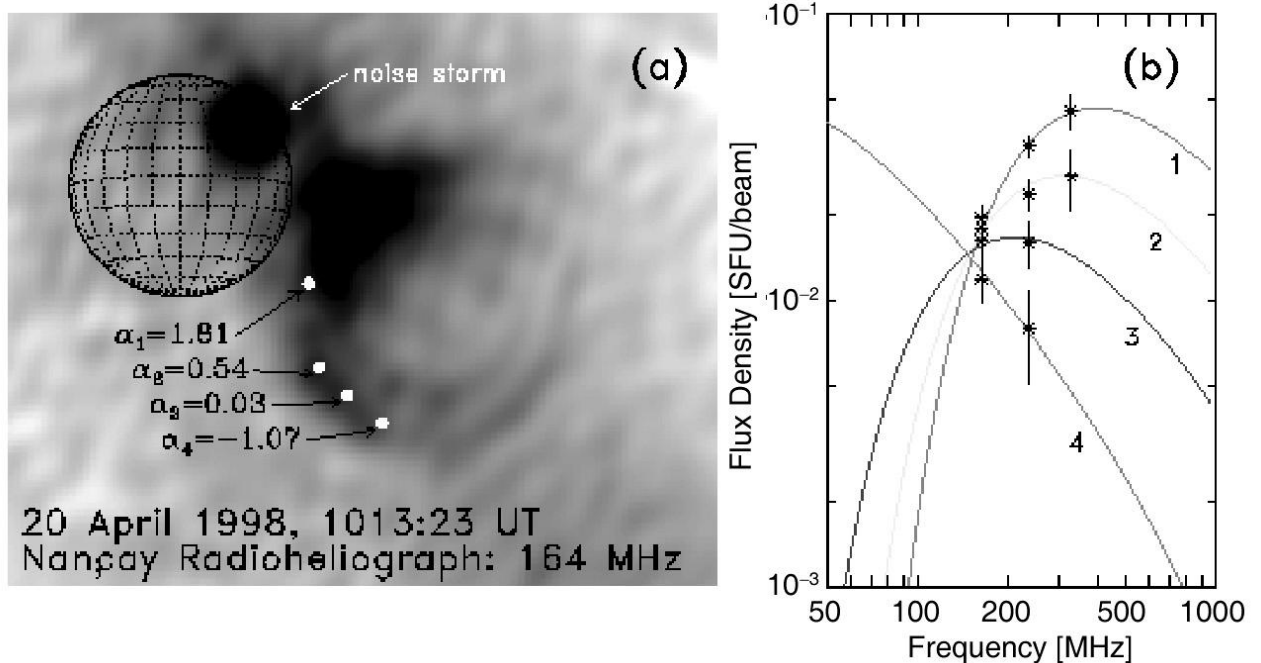


Fig. 7.— Example of a radio CME imaged by the Nancay Radioheliograph at a frequency of 164 MHz. (a) The expanding CME loops, after subtraction of the background Sun. (b) Model fits to multi-frequency spectra taken at the lines of sight indicated in a. Figure adapted from Bastian (2003b).

great number of sources to be imaged. FASR’s snapshot coverage should permit the brighter features of the network to be imaged on short timescales, but it may require significant temporal and frequency-synthesis integration to get down to weaker sources. Detailed modeling will be done to investigate these questions, but FASR is sure to provide many new insights due to the sensitivity of radio emission to temperature, density, and magnetic field in just the height range of greatest interest.

IV. FASR STATUS AND FUTURE PLANS

The Frequency Agile Solar Radiotelescope has been reviewed and recommended for development and funding by three National Research Council (NRC) committees: the 1998 Parker Committee on Groundbased Solar Physics, the 2000 Astronomy and Astrophysics Survey Committee, and the 2002 Solar and Space Physics Survey Committee. The latter decadal survey ranked FASR number 1 in the “small” (>\$150 M) category. A design study and implementation plan is now being readied through a small grant from the Advanced Instrumentation and Technology (ATI) program at the U.S. National Science Foundation. The goal of this study is to have a well-costed design of a system that will work, of sufficient detail that a follow-on proposal can be submitted. Additional funding is expected starting in 2004, leading to the beginning of construction by 2005 or 2006, for completion by 2009.

We have developed an international collaboration with A. Kerdraon and M. Pick, at Obs. Paris, and other European groups in Switzerland and Germany have expressed interest. The main FASR web page is at <http://www.ovsa.njit.edu/fasr/>.

ACKNOWLEDGEMENTS

I would like to thank Prof. Yun and the organizers of the workshop who provided the opportunity for a delightful visit to Seoul National University. I am indebted to Y. Mok for providing the active region model on which section IIIa is based, and to J. Lee for creating an early version of the modeling software. This work is supported by NSF grants AST-0138317 and AST-9987366 to New Jersey Institute of Technology.

REFERENCES

- Aschwanden, M. J. & Benz, A. O. 1997, Electron Densities in Solar Flare Loops, Chromospheric Evaporation Upflows, and Acceleration Sites, *ApJ*, 480, 825
- Bastian, T. S. 1994, Angular scattering of solar radio emission by coronal turbulence, *ApJ*, 426, 774
- Bastian, T. S. 2003a, Frequency agile solar radiotelescope, *Proc. SPIE*, 4853, 98
- Bastian, T. S. 2003b, The frequency agile solar radiotelescope, *Advances in Space Research*, in press
- Bastian, T. S., Benz, A. O., & Gary, D. E. 1998, Radio emission from solar flares, *ARA&A*, 36, 131

- Bastian, T. S., Dulk, G. A., & Leblanc, Y. 1996, High-Resolution Microwave Observations of the Quiet Solar Chromosphere, *ApJ*, 473, 539
- Bastian, T. S. & Gary, D. E. 1997, On the feasibility of imaging coronal mass ejections at radio wavelengths, *J. Geophys. Res.*, 102, 14031
- Bastian, T. S., Gary, D. E., White, S. M., & Hurford, G. J. 1998, Broadband microwave imaging spectroscopy with a solar-dedicated array, *Proc. SPIE*, 3357, 609
- Bastian, T. S., Pick, M., Kerdraon, A., Maia, D., & Vourlidas, A. 2001, The Coronal Mass Ejection of 1998 April 20: Direct Imaging at Radio Wavelengths, *ApJ*, 558, L65
- Boone, F. 2001, Interferometric array design: Optimizing the locations of the antenna pads, *A&A*, 377, 368
- Brosius, J. W., Landi, E., Cook, J. W., Newmark, J. S., Gopalswamy, N., & Lara, A. 2002, Measurements of Three-dimensional Coronal Magnetic Fields from Coordinated Extreme-Ultraviolet and Radio Observations of a Solar Active Region Sunspot, *ApJ*, 574, 453
- Cane, H. V. & Stone, R. G. 1984, Type II solar radio bursts, interplanetary shocks, and energetic particle events, *ApJ*, 282, 339
- Cane, H. V. & Reames, D. V. 1988, Some statistics of solar radio bursts of spectral types II and IV, *ApJ*, 325, 895
- Carlsson, M. & Stein, R. F. 1995, Does a nonmagnetic solar chromosphere exist?, *ApJ*, 440, L29
- Gary, D. E., Dulk, G. A., House, L., Illing, R., Sawyer, C., Wagner, W. J., McLean, D. J., & Hildner, E. 1984, Type II bursts, shock waves, and coronal transients - The event of 1980 June 29, 0233 UT, *A&A*, 134, 222
- Gary, D. E. & Hurford, G. J. 1994, Coronal temperature, density, and magnetic field maps of a solar active region using the Owens Valley Solar Array, *ApJ*, 420, 903
- Gary, D. E. & Keller, C. U. 2003, Site testing issues for the frequency agile solar radiotelescope (FASR), *Proc. SPIE*, 4853, 523
- Gary, D. E. & Zirin, H. 1988, Microwave structure of the quiet sun, *ApJ*, 329, 991
- Gary, D. E., Zirin, H., & Wang, H. 1990, Microwave structure of the quiet sun at 8.5 GHz, *ApJ*, 355, 321
- Gopalswamy, N. & Kundu, M. R. 1992, Estimation of the mass of a coronal mass ejection from radio observations, *ApJ* 390, L37
- Grebinskij, A., Bogod, V., Gelfreikh, G., Urpo, S., Pohjolainen, S., & Shibasaki, K. 2000, Microwave tomography of solar magnetic fields, *A&AS*, 144, 169
- Kathiravan, C., Ramesh, R., & Subramanian, K. R. 2002, Metric Radio Observations and Ray-tracing Analysis of the Onset Phase of a Solar Eruptive Event, *ApJ*, 567, L93
- Krucker, S., Benz, A. O., Bastian, T. S., & Acton, L. W. 1997, X-Ray Network Flares of the Quiet Sun, *ApJ*, 488, 499
- Lee, J., McClymont, A. N., Mikic, Z., White, S. M., & Kundu, M. R. 1998, Coronal Currents, Magnetic Fields, and Heating in a Solar Active Region, *ApJ*, 501, 853
- Mok, Y., Lionello, R., Miki, Z. & Linker, J. A. 2003, Thermal structure of solar active regions in three dimensions, *ApJ*, in preparation
- Nindos, A., Kundu, M. R., White, S. M., Gary, D. E., Shibasaki, K., & Dere, K. P. 1999, Microwave and Extreme Ultraviolet Observations of Solar Polar Regions, *ApJ*, 527, 415
- Sault, R. J. & Conway, J. E. 1999, Multi-Frequency Synthesis, *ASP Conf. Ser.* 180: Synthesis Imaging in Radio Astronomy II, 419
- Shibasaki, K. 1998, Radio Synoptic Maps and Polar Cap Brightening, *ASP Conf. Ser.* 140: Synoptic Solar Physics, 373
- White, S. M. & Kundu, M. R. 1997, Radio Observations of Gyroresonance Emission from Coronal Magnetic Fields, *Sol. Phys.*, 174, 31
- White, S., Lee, J., Aschwanden, M. A., & Bastian, T. S. 2003, Imaging capabilities of the Frequency Agile Solar Radiotelescope (FASR), *Proc. SPIE*, 4853, 531